

Analyst

Accepted Manuscript



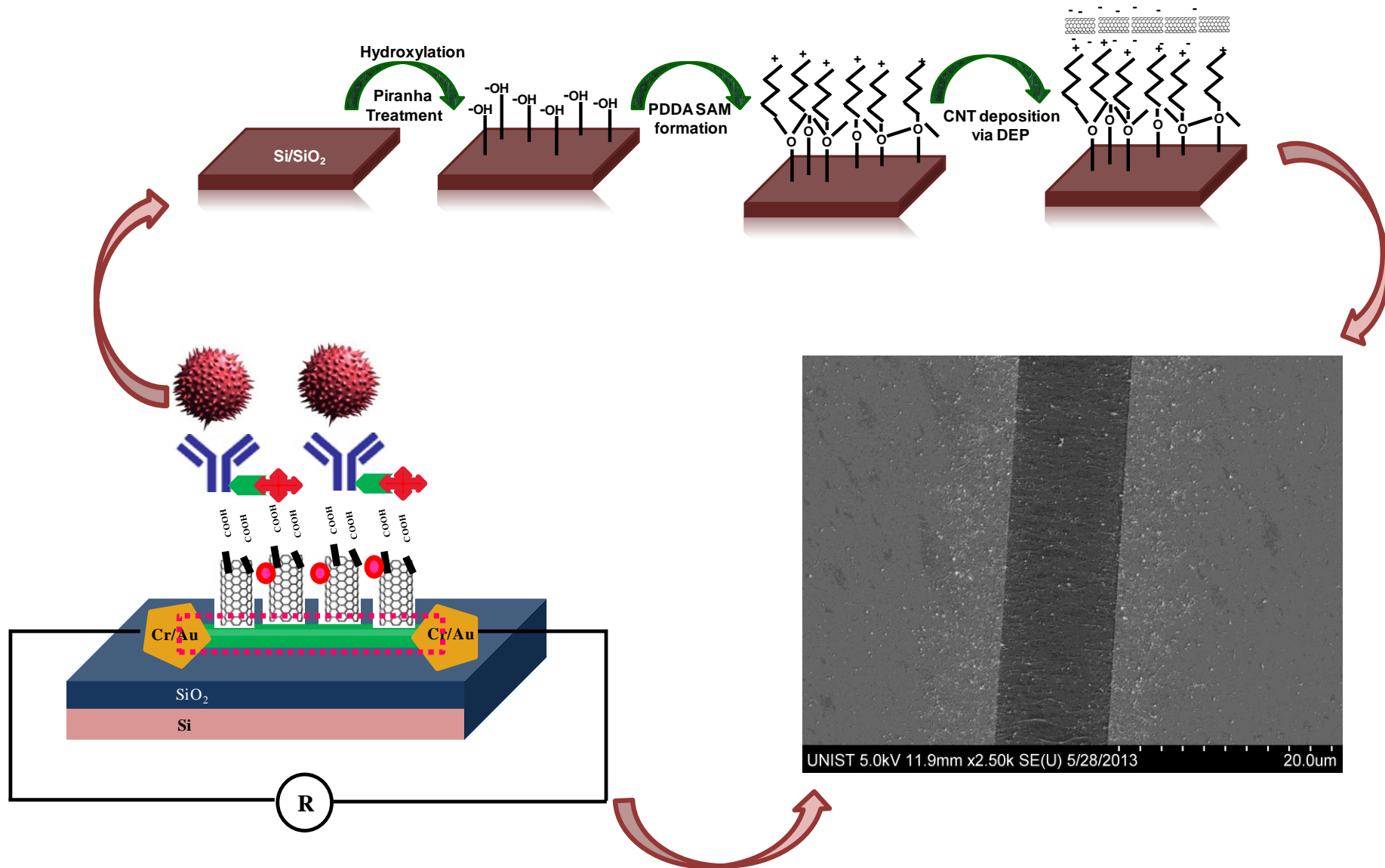
This is an *Accepted Manuscript*, which has been through the Royal Society of Chemistry peer review process and has been accepted for publication.

Accepted Manuscripts are published online shortly after acceptance, before technical editing, formatting and proof reading. Using this free service, authors can make their results available to the community, in citable form, before we publish the edited article. We will replace this *Accepted Manuscript* with the edited and formatted *Advance Article* as soon as it is available.

You can find more information about *Accepted Manuscripts* in the [Information for Authors](#).

Please note that technical editing may introduce minor changes to the text and/or graphics, which may alter content. The journal's standard [Terms & Conditions](#) and the [Ethical guidelines](#) still apply. In no event shall the Royal Society of Chemistry be held responsible for any errors or omissions in this *Accepted Manuscript* or any consequences arising from the use of any information it contains.

Table of contents (TOC)



Analyst Accepted Manuscript

1
2
3
4
5
6
7
8
9
10
11
12
13
14
15
16
17
18
19
20
21
22
23
24
25
26
27
28
29
30
31
32
33
34
35
36
37
38
39
40
41
42
43
44
45
46
47
48
49

1
2
3
4
5 **Electrical Immunosensor based on Dielectrophoretically-deposited**
6 **Carbon Nanotubes for Detection of Influenza Virus H1N1**
7
8

9 Renu Singh^a, Abhinav Sharma^a, Seongkyeol Hong^a, Jaesung Jang^{a,b,c,*}
10
11

12 ^a School of Mechanical and Nuclear Engineering, Ulsan National Institute of Science and
13 Technology (UNIST), Ulsan 689-798, Republic of Korea
14

15 ^b Department of Biomedical Engineering, Ulsan National Institute of Science and
16 Technology (UNIST), Ulsan 689-798, Republic of Korea
17

18 ^c School of Materials Science and Engineering, Ulsan National Institute of Science and
19 Technology (UNIST), Ulsan 689-798, Republic of Korea
20
21
22
23
24
25
26
27
28
29
30
31
32
33
34
35
36
37
38
39
40
41
42
43
44
45
46
47
48
49

50
51 *Correspondence should be addressed to jjang@unist.ac.kr. Tel: +82-52-217-2323 Fax:
52 +82-52-217-2409
53
54
55
56
57
58
59
60

Abstract

The influenza virus has received extensive attention due to the recent swine-origin H1N1 pandemics. This paper reports a label-free, highly sensitive and selective electrical immunosensor for detection of influenza virus H1N1 based on dielectrophoretically deposited single-walled carbon nanotubes (SWCNTs). COOH functionalized SWCNTs were deposited on a self-assembled monolayer of polyelectrolyte polydiallyldimethylammonium chloride (PDDA) between two gold electrodes by the dielectrophoretic and electrostatic forces, making reproducible, uniform, aligned, and aggregation-free SWCNT channels (2-10 μm length). Avidin was immobilized onto the PDDA-SWCNT channels and viral antibodies were immobilized using biotin-avidin coupling. The resistance of the channels increased with the binding of the influenza viruses to the antibodies. These immunosensors showed a linear behavior as the virus concentration was varied from 1 to 10^4 PFU/ml along with a detection time of 30 min. The immunosensors with 2 μm channel length detected 1 PFU/ml of the influenza virus accurately ($R^2=0.99$) and selectively from MS2 bacteriophages. These immunosensors have the potential for a rapid clinical diagnosis component of a point-of-care test kit.

Keywords: Carbon nanotubes; influenza virus; H1N1; immunosensor; dielectrophoresis; PDDA; bacteriophages.

1. Introduction

Continuous outbreaks of highly pathogenic influenza virus H1N1 and many cases of human infection have caused significant international concern. Influenza viruses spread out easily by air transmission and the infection through the respiratory system is quickly done, resulting in an urgent need to detect the influenza virus rapidly and reliably.¹ Conventional virus detection methods such as diagnostic test kits, enzyme-linked immunosorbent assay, and virus isolation and polymerase chain reaction are either poor in specificity, low in sensitivity, time consuming, expensive, or require a laboratory and a trained technician.²⁻⁶ Hence, it is highly desirable to develop a simple, sensitive, and inexpensive sensor to detect the virus rapidly and accurately.⁷

Immunosensors are analytical devices that yield measurable signals in response to specific antigen–antibody interactions, thereby showing a quantity of the antigens in a sample. For virus detection, many immunosensors have been developed using electrochemical,⁸⁻¹⁵ frequency change,¹⁶⁻¹⁸ optical,¹⁹⁻²⁰ and electrical²¹⁻²³ properties. The electrical detection technique has several advantages such as simple and convenient measurements, which enables miniaturized and inexpensive biosensors. Therefore, it has a potential to revolutionize traditional laboratory techniques for virus detection.

1
2
3
4
5
6 Carbon nanotubes (CNTs) have proven to be a promising platform of
7
8
9 ultrasensitive and miniaturized immunosensors for disease diagnosis because of superior
10
11
12 mechanical and conductive properties such as high actuating stresses, low driving voltages,
13
14 and high energy densities.²⁴ However, the development of effective functionalization
15
16
17 methods which can not only introduce homogeneous surface functional groups, but also
18
19
20 cause less or no structural damage to CNTs remains a major challenge.²⁵
21
22
23 Polydiallyldimethylammonium chloride (PDDA)-CNTs has been used in biosensing
24
25
26 applications owing to its good film-forming ability and susceptibility to chemical
27
28
29 modifications.^{26, 27} The strong adsorption of the positively charged PDDA on CNTs may be
30
31
32 due to the π - π interaction between PDDA and the basal plane of graphite of CNTs. This
33
34
35 non-covalent polyelectrolyte functionalization cannot only lead to homogeneous surface
36
37
38 functional groups on CNTs, but also preserves the intrinsic properties of CNTs without
39
40
41 damaging their perfect surface structure.²⁵ The uniformly distributed CNTs realized onto
42
43
44 PDDA can offer much higher surface areas and electrocatalytic activity for virus detection.
45

46
47 Dielectrophoresis (DEP) has been considered one of the reliable, inexpensive, and
48
49
50 efficient CNT deposition techniques and it involves the deposition of solution dispersed
51
52
53 CNTs between electrodes with alignment by applying AC electric fields. Although
54
55
56 chemical vapor deposition (CVD) is a common method for the direct growth of CNTs or a
57
58
59
60

1
2
3
4
5
6 network of CNTs, and CVD-grown CNTs have showed the best performance, the DEP
7
8
9 technique is generally much simpler and more cost-effective, and does not require
10
11
12 specialized materials and high temperature for the growth. Moreover, the alignment and
13
14
15 the density of the deposited CNTs can be controlled by the AC frequency and the
16
17
18 concentration of CNTs.²⁸⁻³⁰
19

20
21 Here, we present a label-free and highly sensitive electrical immunosensor to
22
23
24 detect influenza viruses H1N1 using the single-walled carbon nanotubes (SWCNTs)
25
26
27 deposited on a PDDA self-assembled monolayer (SAM) by DEP. Avidin was immobilized
28
29
30 on the SWCNTs, and viral antibodies were then immobilized using biotin-avidin coupling.
31
32
33 The resistance shift of the SWCNT channels was measured as the concentration of the
34
35
36 virus was varied from 1 to 10^4 PFU/ml, and the selectivity of the immunosensor was also
37
38
39 tested against high concentration MS2 bacteriophages.
40

41
42 In this study, the DEP technique was extended in conjunction with a PDDA SAM
43
44
45 and the piranha treatment, which introduced abundant surface hydroxyl groups (–OH) via
46
47
48 the hydroxylation process. That is, the SWCNTs were deposited by both the
49
50
51 dielectrophoretic and electrostatic forces, which were exerted between the positively
52
53
54 charged –NH₂ groups from PDDA and the negatively charged (–COOH– functionalized)
55
56
57 SWCNTs, resulting in the reproducible, uniform, and aligned SWCNT deposition. This is
58
59
60

1
2
3
4
5
6 the significant difference compared to the previous DEP-deposited CNT sensors for virus
7
8
9 detection. García-Aljaro *et al.*²² developed CNT-based immunosensors for detection of
10
11
12 bacteriophage T7 without a SAM, yielding ~10 MΩ resistance, and the immunosensors
13
14
15 were annealed in order to have good contact. Lee *et al.*³⁰ presented CNT-based influenza
16
17
18 virus immunosensors by the layer-by-layer assembly method, which culminated in a
19
20
21 random, broken, and dense network of SWCNTs, where tube-tube junction may limit
22
23
24 charge transport.
25
26
27
28

29 **2. Materials and methods**

30 **2.1. Biomolecules and chemical reagents**

31
32
33 CNTs (90% of SWCNTs, diameter: 1–2 nm, length: 5–30 μm, COOH content:
34
35 ~2.75 wt%) were purchased from M K Impex Corp. (Canada). PDDA (20 wt%, MW =
36
37
38 200–350k), avidin (A9275), bovine serum albumin (BSA) (A2153), N-(3-
39
40
41 Dimethylaminopropyl)-N'-ethylcarbodiimide hydrochloride (EDC) (03449), N-
42
43
44 Hydroxysuccinimide (NHS) (130672), glutaraldehyde (G765), osmium tetroxide (75632),
45
46
47 and isoamylacetate (112674) were obtained from Sigma–Aldrich (USA).
48
49
50
51
52 Dimethylformamide (DMF) (98%, D1021) and phosphate buffer saline (PBS) (1X, pH
53
54
55 7.4) containing 0.1% Tween 20 (P2006) were purchased from Biosesang Inc. (South
56
57
58
59
60

1
2
3
4
5
6 Korea). PBS (10X, pH 7.4, 70011-044) was purchased from Invitrogen Life Technologies
7
8
9 (USA). Biotin conjugated mouse anti-influenza A monoclonal antibody (bs-1261M) was
10
11
12 purchased from Gentaur molecular products (USA). Influenza virus H1N1 (KBPV-VR-
13
14 33) was procured from the Bank of Pathogenic Viruses (South Korea). Bacteriophage
15
16 MS2 (ATCC® 15597-B1™, 1×10^9 PFU/ml) was procured from Koram Biogen Corp.
17
18 (South Korea). Deionized water (dH₂O) (resistance: ~18.2 MΩ) from the Millipore water
19
20
21 purification system was utilized for preparation of the desired aqueous solutions
22
23
24 (molecular biology grade). All the solutions and glassware were autoclaved prior to being
25
26
27 used.
28
29
30
31
32
33
34

35 2.2. Microelectrode fabrication

36
37
38 A standard 6 inch silicon (Si) wafer with thermally grown silicon dioxide (SiO₂,
39
40 thickness: 500 nm) was cleaned with a piranha solution (H₂SO₄:H₂O₂ = 2:1) at room
41
42 temperature for 15 min, rinsed thoroughly with a copious amount of dH₂O, and dried with
43
44 a nitrogen gas stream. Two electrodes for the source and the drain were patterned using
45
46 photolithography, and then chromium (thickness: 20 nm) and gold (thickness: 200 nm)
47
48 were electron beam evaporated sequentially onto the Si/SiO₂ substrate. The source and the
49
50 drain electrodes were tapered as shown in Fig. 1 to maximize the electric field at the edges
51
52
53
54
55
56
57
58
59
60

1
2
3
4
5
6 and to increase the amount of uniformly distributed SWCNT connections during the DEP
7
8
9 assembly. The gaps, which are referred to as channel lengths, between these two
10
11 electrodes were 2 μm , 5 μm , and 10 μm and the width of the facing electrodes was 100
12
13 μm . The silicon wafer was then diced into chips (10 mm \times 10 mm). The chips were
14
15 cleaned in piranha solution followed by rinsing with dH_2O . These chips were then dried
16
17
18 with nitrogen gas and either used immediately or stored under vacuum in a desiccator.
19
20
21
22
23
24
25

26 **2.3. DEP assembly of SWCNT channels**

27
28

29 Firstly, a SAM of PDDA was made as a precursor layer by pipetting onto the
30
31 channel area for the charge enhancement and incubating for 15 min at 25°C prior to the
32
33 DEP deposition step. A SWCNT suspension was prepared by suspending the SWCNTs in
34
35 DMF (10 $\mu\text{g}/\text{ml}$) by sonication in a water bath for 90 min followed by centrifugation at
36
37 5,000 rpm for 1 h, and the supernatant liquid was discarded. The remaining SWCNT
38
39 suspension can be kept for at least 1 month, and a 10 min sonication step is necessary
40
41 before each use. The DEP assembly of the SWCNTs was performed by dropping 20 μl of
42
43 the SWCNT suspension onto the channel area, and applying 10 V (peak to peak value) at
44
45 200 kHz for few sec. Finally, a thin film of uniformly distributed, parallelly aligned, and
46
47
48
49
50
51
52
53
54
55
56
57
58
59
60

1
2
3
4
5
6 aggregation-free SWCNTs was formed as a channel between the source and the drain
7
8
9 electrodes. The chips were then rinsed with DMF, dH₂O followed by mild N₂ drying.
10

11 12 13 14 15 **2.4. Immunofunctionalization and virus attachment** 16

17
18 Firstly, 90 μ l of avidin (1 mg/ml) was mixed with 5 μ l of EDC (15 mM) and 5 μ l
19
20 of NHS (30 mM), and the mixture was incubated for 2 h at 25°C. Avidin was then
21
22 immobilized onto the SWCNTs by depositing 10 μ l of the mixture and incubating for 30
23
24 min. The SWCNT channels were washed with dH₂O and subjected to 10 μ l of biotinylated
25
26 monoclonal antibodies (10 μ g/ml) specific to influenza virus H1N1 in an incubator at 37
27
28 °C for 2 h. After washing with PBS (1X, pH 7.4), the SWCNT channels were incubated
29
30 for 30 min in BSA (1 mg/ml) to prevent nonspecific binding followed by washing with
31
32 PBS (1X, pH 7.4) containing 0.1% Tween 20 to remove loosely attached PDDA and
33
34 SWCNTs. The immunosensors were then incubated in 10 μ l of various concentrations of
35
36 the viruses in PBS (1X, pH 7.4) for 30 min followed by rinsing, air-drying and resistance
37
38 measurement. The influenza viruses were inactivated using Ultraviolet Crosslinker (CL-
39
40 1000 UV crosslinker, UVP, Upland, CA, USA) prior to being used. A schematic of the
41
42 developed SWCNT immunosensor and its test set-up are shown in Fig. 1. The selectivity
43
44 of the immunosensor was assessed by incubating the immunosensor with high
45
46
47
48
49
50
51
52
53
54
55
56
57
58
59
60

1
2
3
4
5
6 concentration MS2 bacteriophages and measuring the resistance change due to the binding
7
8
9 to the SWCNT channels.

10 11 12 13 14 15 **2.5. Electrical measurements**

16
17
18 The electrical measurement of the immunosensors was conducted by collecting
19
20 the current-voltage (I–V) data from the immunosensors. The immunosensor response due
21
22 to the virus attachment was measured as the normalized increase in resistance (NIR), $[\Delta R$
23
24 $= (R_{\text{Virus}} - R)]/R$, where R_{Virus} is the resistance of the immunosensor after the exposure to
25
26 the viruses and R is the immunosensor resistance after the antibody immobilization. The
27
28 resistance of the immunosensors was measured after every functionalization step. The
29
30 applied voltage was varied from -1.0 to $+1.0$ V, and current was recorded using a Source
31
32 Meter® (2400, Keithley, Cleveland, OH).
33
34
35
36
37
38
39
40
41
42

43 44 **2.6. Morphological and structural characterizations**

45
46 Atomic force microscopy (AFM) and scanning electron microscopy (SEM) were
47
48 used for morphological characterizations of the immunosensors. AFM images were
49
50 obtained using a (Dimension) AFM 3100 (Veeco, USA). The chemical fixation was
51
52 performed to image the influenza viruses captured on the SWCNT channel. First, the
53
54
55
56
57
58
59
60

1
2
3
4
5
6 immunosensors were immersed in 2.5% glutaraldehyde for 2 h and washed in 1X PBS
7
8
9 buffer for 10 min. They were then immersed in 1% osmium tetroxide in distilled water for
10
11
12 2 h and washed again in 1X PBS buffer twice for 10 min each. The immunosensors were
13
14
15 then placed in 25, 50, 70, 90, 100, and 100 % ethanol sequentially for 10 min each for
16
17
18 dehydration. They were treated with a mixture of isoamylacetate and ethanol at a ratio of
19
20
21 1:3, 1:1, 1:0, and 1:0 sequentially for 10 min each for infiltration. The immunosensors
22
23
24 were then placed in a critical point dryer (SPI Supplies) at 35°C at 1200 psi and coated
25
26
27 with a thin layer of platinum for imaging with a scanning electron microscope (s-4800,
28
29
30 Hitachi). A Fourier transform infrared (FT-IR) Varian 4100 (Agilent, USA) instrument was
31
32
33 used for structural characterization without any further treatment of the samples
34
35
36 (Supplementary data and supplementary Fig 1).
37
38
39
40

41 **3. Results and Discussion**

42 **3.1. Morphological characterization - SEM**

43
44
45
46 Fig. 2 a and b show SEM images of the uniformly distributed, aligned, and
47
48
49 aggregation-free SWCNTs after the PDDA SAM and DEP assembly, demonstrating that
50
51
52 the majority of the individual SWCNTs were reasonably aligned in parallel to the
53
54
55 electrodes along with a few mis-aligned and tilted nanotubes. These aligned SWCNTs
56
57
58
59
60

1
2
3
4
5
6 contrast with a non-aligned and dense network of SWCNTs made by sedimentation (Fig.
7
8
9 2c). The PDDA SAM also helped the reproducibility of the deposition. This reproducible
10
11 formation of uniform and aligned SWCNTs can be attributed to the combined effects of the
12
13 DEP assembly and the SAM treatment. From these images, the average linear density of
14
15 SWCNT arrays were estimated to be ~ 8 SWCNT/ μm , which may strongly influence the
16
17 performance of the fabricated SWCNT immunosensor.³¹ After the avidin and biotinylated
18
19 antibody immobilization, uniform morphology appeared due to the interaction of avidin
20
21 with the carboxyl functionalized SWCNT surfaces and biotinylated antibodies, revealing
22
23 the successful immobilization of avidin and biotinylated antibodies onto the SWCNT
24
25 surfaces (Fig. 2 d). Fig. 2 e shows a single influenza virus captured by the antibodies that
26
27 were distributed on the SWCNTs, with several virus aggregates observed as well. The
28
29 diameter of a single influenza virus was reported to be 80-120 nm,³² and previous studies
30
31 have shown that the SWCNTs functionalized with specific antibodies were able to capture
32
33 viruses.²³
34
35
36
37
38
39
40
41
42
43
44
45
46
47
48
49

50 **3.2. Morphological characterization - AFM**

51
52 Fig. 3 illustrates the schematic of the SWCNT deposition after the PDDA SAM
53
54 formation along with the AFM micrographs of (a) PDDA, (b) PDDA-SWCNT, and (c)
55
56
57
58
59
60

1
2
3
4
5
6 PDDA-SWCNT-Avidin-biotinylated antibody. An initial monolayer of PDDA adsorbed
7
8
9 was relatively smooth with surface roughness of 1.27 nm (Fig. 3 a). Fig. 3 b exhibits a
10
11
12 layer of the DEP-deposited SWCNTs with an increased surface roughness of 80.2 nm. Fig.
13
14
15 3 c shows an AFM image after the antibody was covalently linked onto the SWCNTs
16
17
18 using avidin-biotin coupling. The spiky nanotube features disappeared, and a globular
19
20
21 surface generally reminiscent of thin antibody coatings was seen.³³ It is clearly visible
22
23
24 from Fig. 3 c that a remarkable decrease in surface roughness (15.4 nm) was a result of
25
26
27 antibody attachment.
28
29
30

31 **3.3. Resistance measurements and incubation time dependency**

32
33
34 Fig. 4 a shows the resistance measurement of the immunosensors after PDDA-
35
36
37 SWCNT deposition for various channel lengths of 2, 5 and 10 μm . The resistance was
38
39
40 found to increase linearly with the channel length demonstrating a relationship of $R = 9.97$
41
42
43 $\times L + 10.8$, where R and L are expressed in $\text{k}\Omega$ and μm , respectively. The measurements
44
45
46 also showed good repeatability, where the relative variations of the measurements were
47
48
49 $\sim 3\%$. García-Aljaro *et al.*²² presented $\sim 10 \text{ M}\Omega$ resistance for DEP-deposited SWCNTs,
50
51
52 and the chips were annealed in order to have good contact. We used PDDA as a precursor
53
54
55 for the charge enhancement and achieved 1-100 $\text{k}\Omega$ for a thin film of uniformly
56
57
58 distributed, aligned, and aggregation-free SWCNTs at 2-10 μm channel lengths. I-V
59
60

1
2
3
4
5
6 characteristics for the SWCNT immunosensors were shown in the supplementary data and
7
8
9 supplementary Fig. 2.

10
11 The next experiment was focused on determining the required incubation time for
12
13 maximum resistance change because the resistance can increase with the attachment of
14
15 analytes. To this end, the SWCNT immunosensors were incubated in 10^4 PFU/mL of
16
17 influenza viruses at room temperature, and NIR was measured with incubation time. Fig. 4
18
19 b shows that the NIR increased with incubation time up to 30 min attaining a plateau value
20
21 of 1.5 with respect to the initial resistance. Accordingly, 30 min incubation time was used
22
23
24
25
26
27
28
29
30
31
32
33
34
35 in the subsequent experiments.

3.4. Resistance measurements after each functionalization

36
37
38 The resistance measurements of the SWCNT immunosensors were performed
39
40 after each step of the functionalization: PDDA-SWCNT, avidin, antibodies, and H1N1
41
42 virus (10^2 PFU/ml) (Fig. 5 a). The antibodies immobilized on the avidin did not change
43
44 the resistance as much as avidin did on the PDDA-SWCNTs. According to the
45
46 measurements, there must be an electrostatic and/or structural change to induce observable
47
48
49
50
51
52
53
54
55
56
57
58
59
60 resistance shift when avidin was immobilized on the SWCNT surfaces.³⁴ This suggests
that the resistance changes after the immobilization of influenza viruses were probably due

1
2
3
4
5
6 to their charge carrier donating/accepting property and/or the structural change of the
7
8
9 SWCNTs due to the huge structure of the viruses. That is, the attachment of the viruses
10
11 significantly influenced the electrical properties of the SWCNTs to increase resistivity.
12
13

14 15 16 17 18 **3.5. Selectivity and sensitivity**

19
20 To investigate the selectivity of the SWCNT immunosensors, MS2 bacteriophages
21
22 with high concentration (10^9 PFU/ml) were used with 2, 5 and 10 μm channel length chips
23
24 (Fig. 5 b). The averages and standard deviations were determined from 4 sets of
25
26 immunoassay. The NIRs for MS2 bacteriophages were 0.093, 0.148, 0.188 for 2, 5 and 10
27
28 μm channel lengths, respectively, while the NIRs for influenza viruses (10^2 PFU/ml) were
29
30 0.899, 1.79, and 4.95 for 2, 5 and 10 μm channel lengths, respectively. The NIRs due to
31
32 the MS2 bacteriophage attachment were 10-4% of those due to the influenza virus
33
34 attachment even with much higher concentration of MS2 bacteriophages. This test showed
35
36 that the SWCNT immunosensors were highly specific to influenza viruses against MS2
37
38 bacteriophages.
39
40
41
42
43
44
45
46
47
48

49 Fig. 6 shows the calibration plots of the immunosensors as the influenza virus
50
51 concentration was varied from 1 to 10^4 PFU/ml. The higher the influenza virus
52
53 concentration, the larger the resistance shifts due to more influenza viruses adsorbed on
54
55
56
57
58
59
60

1
2
3
4
5
6 the channel surface. The immunosensor response, NIR, was a linear function of logarithm
7
8
9 of viral concentrations between 1 and 10^4 PFU/ml ($R^2 = 0.99, 0.94,$ and 0.89 for 2, 5, and
10
11
12 $10\ \mu\text{m}$ channel lengths, respectively). The immunosensor linearity or accuracy decreased
13
14
15 as the channel length increased. In fact, it was reported that longer channel chips showed
16
17
18 larger measurement variations due to the attachment of other molecules in a virus solution
19
20
21 on open binding sites.³⁰ On the other hand, the longer SWCNT channel chips showed
22
23
24 larger increase in the NIR with the increasing virus concentration, and they have larger
25
26
27 sensing areas, both of which are favorable for a biosensing platform.

28
29
30 According to the measurements, the shortest channel immunosensor was the most
31
32
33 precise and accurate. In fact, the NIR for highly concentrated MS2 bacteriophages was
34
35
36 0.093 while the NIR showed 0.17 for $1\ \text{PFU/ml}$ of the influenza viruses. Moreover, the
37
38
39 NIR for PBS buffer (1X, pH 7.4) showed 0.05 . That is, this immunosensor can detect 1
40
41
42 PFU/ml of the influenza virus selectively from MS2 bacteriophages. This is highly
43
44
45 sensitive considering that the range of influenza viral particles found in the infected swine
46
47
48 nasal samples is $10^3 - 10^5\ \text{TCID}_{50}/\text{ml}$ (50% tissue culture infective dose) and a limit of
49
50
51 detection of $\sim 10^2\ \text{TCID}_{50}/\text{ml}$ was reported recently.³⁰ García-Aljaro *et al.*²² showed a limit
52
53
54 of detection of $10^3\ \text{PFU/ml}$ for bacteriophages T7 using SWCNT-based immunosensors.
55
56
57 Enhanced limit of detection in the present study may be attributed to uniformly distributed,
58
59
60

1
2
3
4
5
6 aligned, and aggregation-free SWCNTs. The reproducible generation of uniform and
7
8 aligned SWCNTs on a PDDA SAM by the dielectrophoretic and electrostatic forces can
9
10 have important implication for the large-scale fabrication of SWCNT-based biosensors.
11
12
13
14
15
16
17

18 **4. Conclusions**

19
20 In this study, we demonstrated a label-free, highly sensitive and selective
21
22 electrical immunosensor to detect whole influenza viruses using dielectrophoretically
23
24 deposited SWCNTs. The reproducible formation of a uniform, aligned, and aggregation-
25
26 free SWCNT thin film between the source and the drain electrodes was observed on a
27
28 PDDA SAM by applying both the dielectrophoretic and electrostatic forces, which showed
29
30 an advantage over applying either as in previous studies. This immunosensor showed a
31
32 linear behavior from 1 to 10^4 PFU/ml along with a detection time of 30 min. The shortest
33
34 channel (2 μm length) immunosensor can detect 1 PFU/ml of the influenza virus
35
36 selectively from MS2 bacteriophages. This SWCNT-based electrical immunosensor has
37
38 potential applications as a point-of-care test kit for rapid and simple clinical diagnosis or a
39
40 component of a portable lab-on-a-chip system.
41
42
43
44
45
46
47
48
49
50
51
52
53
54

55 **Acknowledgments**

56
57
58
59
60

1
2
3
4
5
6
7
8
9
10
11
12
13
14
15
16
17
18
19
20
21
22
23
24
25
26
27
28
29
30
31
32
33
34
35
36
37
38
39
40
41
42
43
44
45
46
47
48
49
50
51
52
53
54
55
56
57
58
59
60

This research was supported by Basic Science Research Program through the National Research Foundation of Korea (NRF) funded by the Ministry of Education, Science and Technology (2012R1A2A2A01012528).

Analyst Accepted Manuscript

References

1. L.T. Kao, L. Shankar, T.G. Kang, G. Zhang, G.K.I. Taym, S.R.M. Rafei and C.W.H. Lee, *Biosens. Bioelectron.*, 2011, **26**, 2006–2011.
2. B. Leuwerke, P. Kitikoon, R. Evans and E. Thacker, *J. Vet. Diagn. Invest.*, 2008, **20**, 426–432.
3. Q.G. He, S. Velumani, Q.Y. Du, C.W. Lim, F.K. Ng, R. Donis and J. Kwang, *Clin. Vaccine Immunol.*, 2007, **14**, 617–623.
4. M.B. Townsend, E.D. Dawson, M. Mehlmann, J.A. Smagala, D.M. Dankbar, C.L. Moore, C.B. Smith, N.J. Cox and R.D. Kuchta, *J. Clin. Microbiol.*, 2006, **44**, 2863–2871.
5. Y. Amano and Q. Cheng, *Anal. Bioanal. Chem.*, 2005, **381**, 156–164.
6. B.W. Lee, R.F. Bey, M.J. Baarsch and R.R. Simonson, *J. Vet. Diagn. Invest.*, 1993, **5**, 510–515.
7. WHO, Geneva, Switzerland. September 2006, 21–22.
8. F. Li, R. Zhou, K. Zhao, H. Chen and Y. Hu, *Talanta*, 2011, **87**, 302–306.
9. Y. Li, M. Hong, Y. Lin, Q. Bin, Z. Lin, Z. Cai and G. Chen, *Chem. Commun.*, 2012, **48**, 6562–6564.

- 1
2
3
4
5
6 10. R. Wang, Y. Wang, K. Lassiter, Y. Li, B. Hargis, S. Tung, L. Berghman and W.
7
8
9 Bottje, *Talanta*, 2009, **79**, 159–164.
10
11
12 11. D. Tang, J. Tang, B. Su, J. Ren and G. Chen, *Biosens. Bioelectron.*, 2010, **25**, 1658–
13
14 1662.
15
16
17 12. R.E. Ionescu, S. Cosnier, G. Herzog, K.G.B. Leshem, S. Herrmann and R.S. Marks,
18
19
20 *Enzyme and Microbial Technology*, 2007, **40**, 403–408.
21
22
23 13. C. Ma, G. Xie, W. Zhang, M. Liang, B. Liu and H. Xiang, *Microchim Acta*, 2012,
24
25
26 **178**, 331–340.
27
28
29 14. N.M.M. Pires, T. Dong, Z. Yang, N. Høivik and X. Zhao, *J. Micromech. Microeng.*,
30
31
32 2011, **21**, 115031.
33
34
35 15. B.T.T. Nguyen, A.E.K. Peh, C.Y. L. Chee, K. Fink, V.T.K. Chow, M.M.L. Ng and
36
37
38 C.S. Toh, *Bioelectrochemistry*, 2012, **88**, 15–21.
39
40
41 16. T.W. Owen, R.O. Alkaysi, C.J. Bardeen and Q. Cheng, *Sensors and Actuators B*,
42
43
44 2007, **126**, 691–699.
45
46
47 17. D. Li, J. Wang, R. Wang, Y. Li, D. Abi Ghanem, L. Berghman, B. Hargis and H. Lu,
48
49
50 *Biosens. Bioelectron.*, 2011, **26**, 4146–4154.
51
52
53 18. S.A. Miller, L.A. Hiatt, R.G. Keil, D.W. Wright and D.E. Cliffler, *Anal.*
54
55
56 *Bioanal. Chem.*, 2011, **399**, 1021–1029.
57
58
59
60

- 1
2
3
4
5
6 19. C.H. Weng, T.B. Huang, C.C. Huang, C.S. Yeh, H.Y. Lei and G.B. Lee, *Biomed.*
7
8
9 *Microdevices*, 2011, **13**, 585–595.
10
11
12 20. S. Kumbhat, K. Sharma, R. Gehlot, A. Solanki and V. Joshi, *Journal of*
13
14 *Pharmaceutical and Biomedical Analysis*, 2010, **52**, 255–259.
15
16
17 21. D.J. Shirale, M.A. Bangar, M. Park, M.V. Yates, W. Chen, N.V. Myung and A.
18
19
20
21
22 Mulchandani, *Environ. Sci. Technol.*, 2010, **44**, 9030–9035.
23
24 22. C. García-Aljaro, L.N. Cella, D.J. Shirale, M. Park, F.J. Muñoz, M.V. Yates and
25
26
27
28 A. Mulchandani, *Biosens. Bioelectron.*, 2010, **26**, 1437–1441.
29
30 23. M. Bhattacharya, S. Hong, D. Lee, T. Cui and S.M. Goyal, *Sensors and Actuators*
31
32
33
34
35
36 24. J.V. Veetil and K. Ye, *Biotechnol Prog.*, 2007, **23**, 517–53.
37
38 25. S. Wang, S.P. Jiang and X. Wang. *Nanotechnology*, 2008, **19**, 265601, 6pp.
39
40
41 26. Y.L. Yao and K.K. Shiu, *Electroanalysis*, 2008, **20**, 1542–1548.
42
43
44 27. S. Srivastava, V. Ball, P. Podsiadlo, J. Lee, P. Ho and N.A. Kotov, *J. Am. Chem.*
45
46
47
48 *Soc.*, 2008, **130**, 3748–3749.
49
50 28. L. Liu, X. Ye, K. Wu, R. Han, Z. Zhou and T. Cui, *Sensors*, 2009, **9**, 1714–
51
52
53
54
55
56
57
58
59
60

- 1
2
3
4
5
6 29. J. Moscatello, V. Kayastha, A. Pandey, B. Ulmen and Y.K. Yap, *Mater. Res. Soc.*
7
8
9 *Symp. Proc. Materials Research Society*, 2008, **1057**, II15–07.
10
11
12 30. D. Lee, Y. Chander, S.M. Goyal and T. Cui, *Biosens. Bioelectron.*, 2011, **26**, 3482–
13
14 3487.
15
16
17 31. B.K. Sarker, S. Shekhar and Saiful I. Khondaker, *ACS nano*, 2011, **5**, 6297–6305.
18
19
20 32. A.M. King, E. Lefkowitz, M.J. Adams, E.B. Carstens, Academic Press, London,
21
22 2011.
23
24
25
26 33. J. F. Rusling and Z. Zhang, in *Handbook Of Surfaces And Interfaces Of Materials*,
27
28 ed. R. W. Nalwa, Academic Press, San Diego, 2001, **5**.
29
30
31 34. I. Heller, A.M. Janssens, J. Malinik, E.D. Minot, S.G. Lema and C. Dekker, *Nano*
32
33 *Lett.*, 2008, **8**, 591–595.
34
35
36
37
38
39
40
41
42
43
44
45
46
47
48
49
50
51
52
53
54
55
56
57
58
59
60

Figure Captions:

Fig. 1 Schematic illustration of the single walled carbon nanotube based immunosensor for H1N1 virus detection. The inset shows an optical image of dielectrophoretically deposited SWCNTs onto a PDDA SAM.

Fig. 2 SEM images of (a) PDDA-SWCNT, (b) PDDA- SWCNT at higher magnification, (c) SWCNTs deposited by sedimentation, (d) H1N1 antibody immobilized PDDA-SWCNT, and (e) H1N1 antibody immobilized PDDA-SWCNT after capturing a single influenza virus.

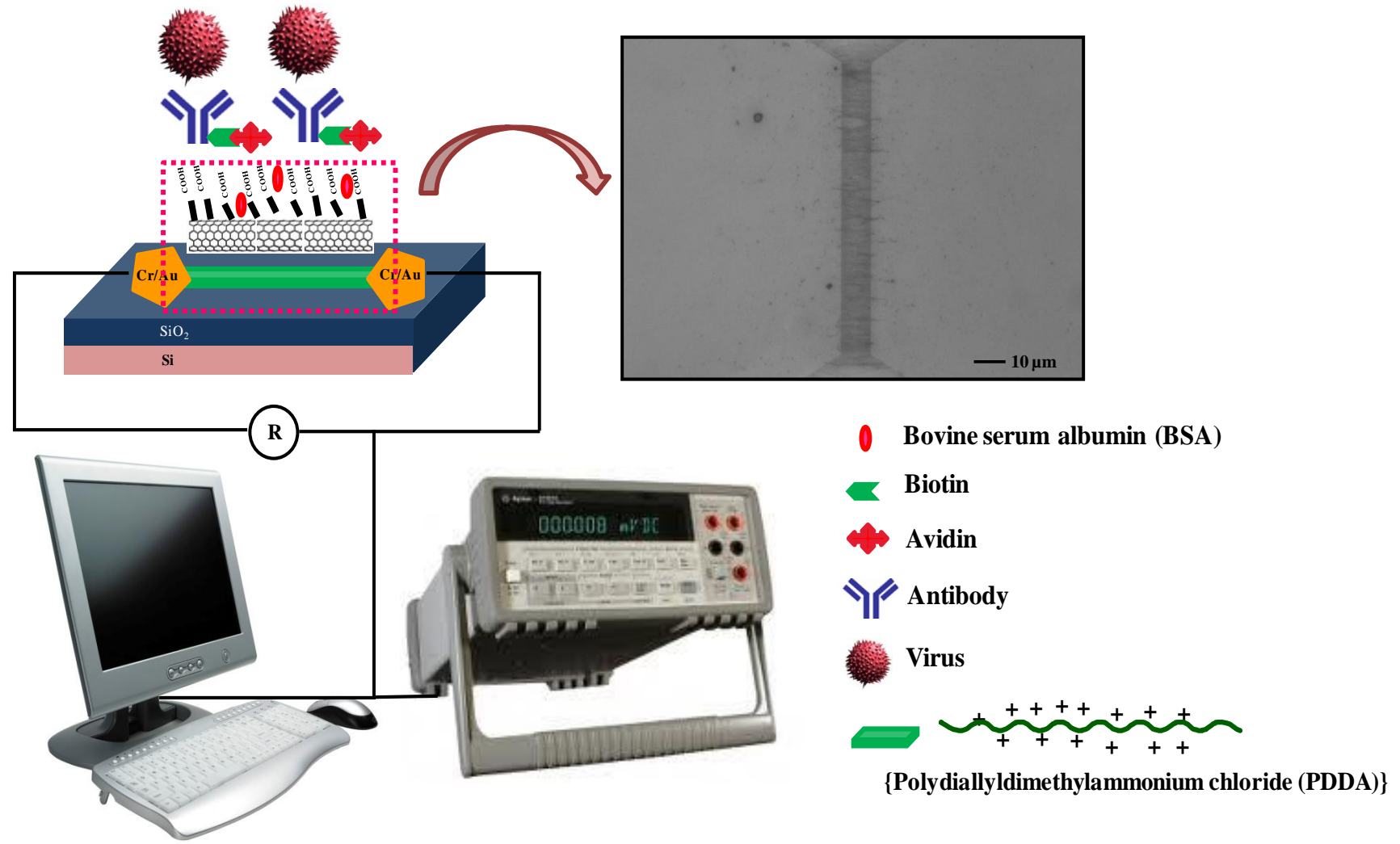
Fig. 3 Schematic of PDDA and SWCNT interaction along with representative AFM (tapping mode) images of (a) PDDA, (b) PDDA-SWCNT, and (c) H1N1 antibody immobilized PDDA-SWCNT.

Fig. 4 (a) Resistance of the PDDA-SWCNT with various channel lengths of 2, 5, and 10 μm and constant width of 100 μm , and (b) Time-dependent response of the PDDA-SWCNT immunosensors after exposure to H1N1 virus (10^4 PFU/mL) with channel length of 2 μm and width 100 μm . The error bars indicate standard deviations from 4 sets of measurements.

Fig. 5 (a) Surface binding studies of PDDA-SWCNT, avidin, biotinylated antibody, and H1N1 virus (10^2 PFU/ml) for various channel lengths of 2, 5, and 10 μm with constant width of 100 μm . (b) Selectivity tests of the SWCNT immunosensor against MS2 bacteriophages (10^9 PFU/ml). The error bars indicate standard deviations from 4 sets of measurements.

Fig. 6 Calibration plots of the SWCNT immunosensors showing that NIRs increased with the logarithm of the virus concentrations, where the channel length was 2, 5, and 10 μm . The error bars indicate standard deviations of 4 sets of measurements. X and Y represent the virus concentration and the NIR, respectively. The NIR showed 0.05 for PBS buffer (1X, pH 7.4).

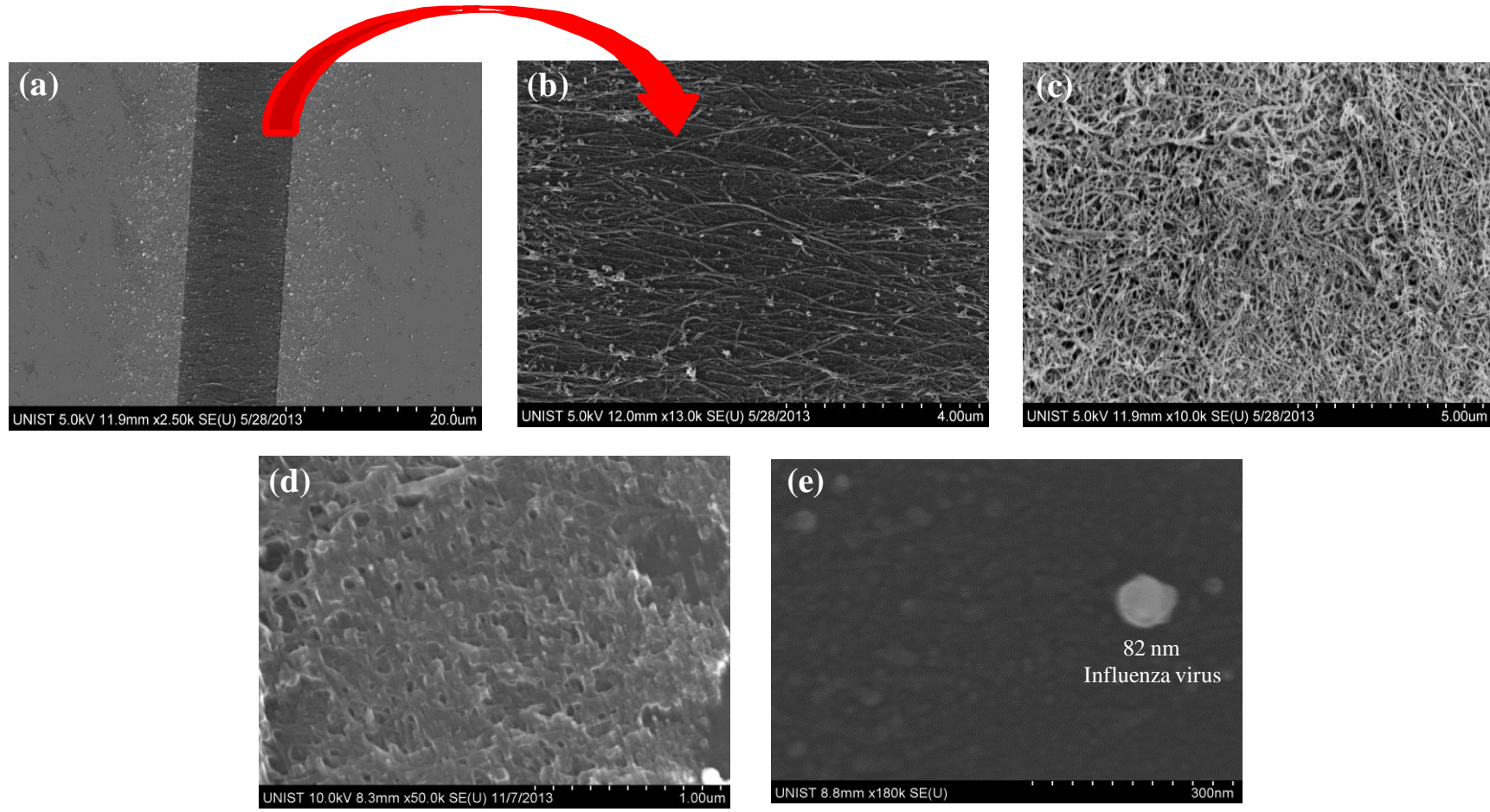
Figure 1



Analyst Accepted Manuscript

1
2
3
4
5
6
7
8
9
10
11
12
13
14
15
16
17
18
19
20
21
22
23
24
25
26
27
28
29
30
31
32
33
34
35
36
37
38
39
40
41
42
43
44
45
46
47
48
49

Figure 2



1
2
3
4
5
6
7
8
9
10
11
12
13
14
15
16
17
18
19
20
21
22
23
24
25
26
27
28
29
30
31
32
33
34
35
36
37
38
39
40
41
42
43
44
45
46
47
48
49

Figure 3

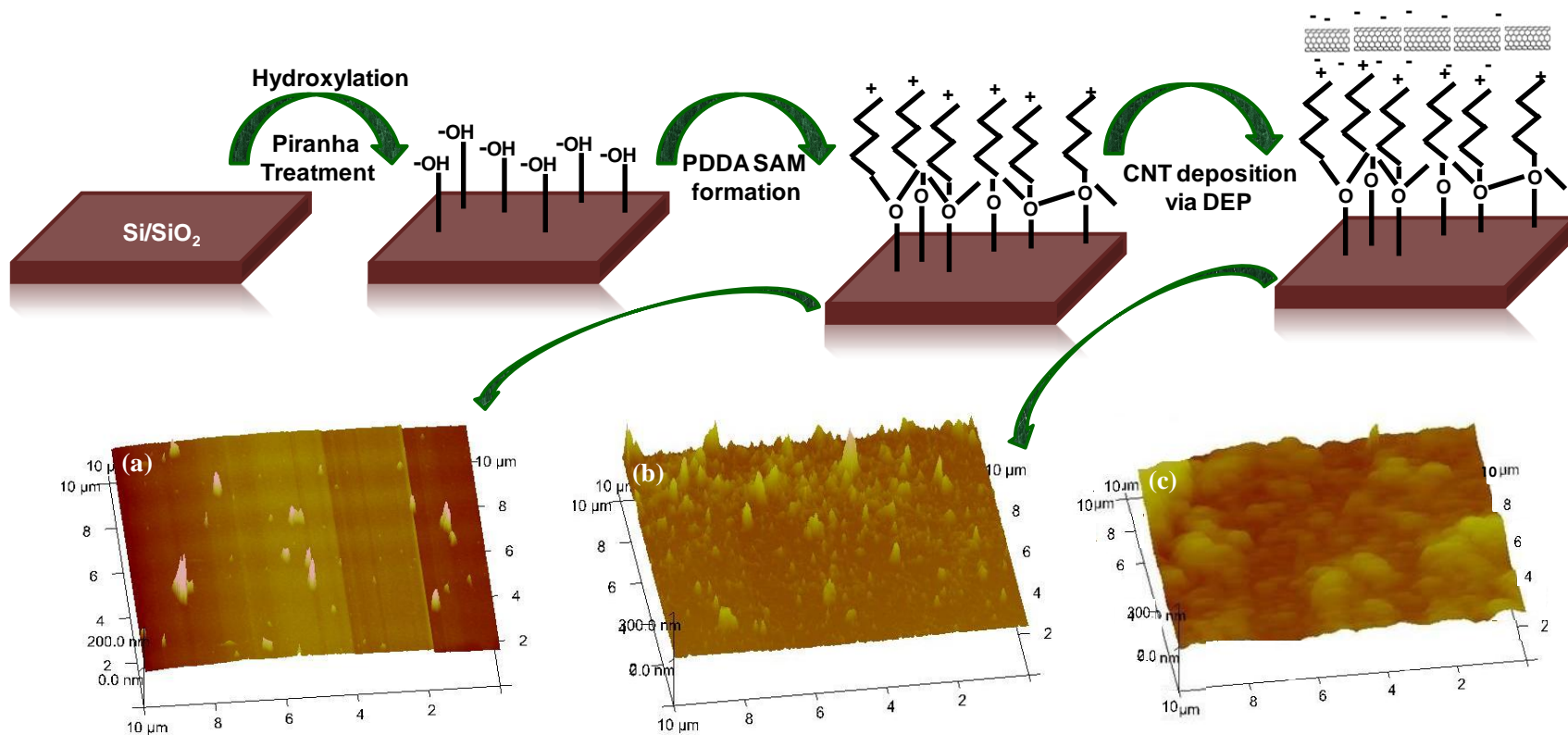


Figure 4

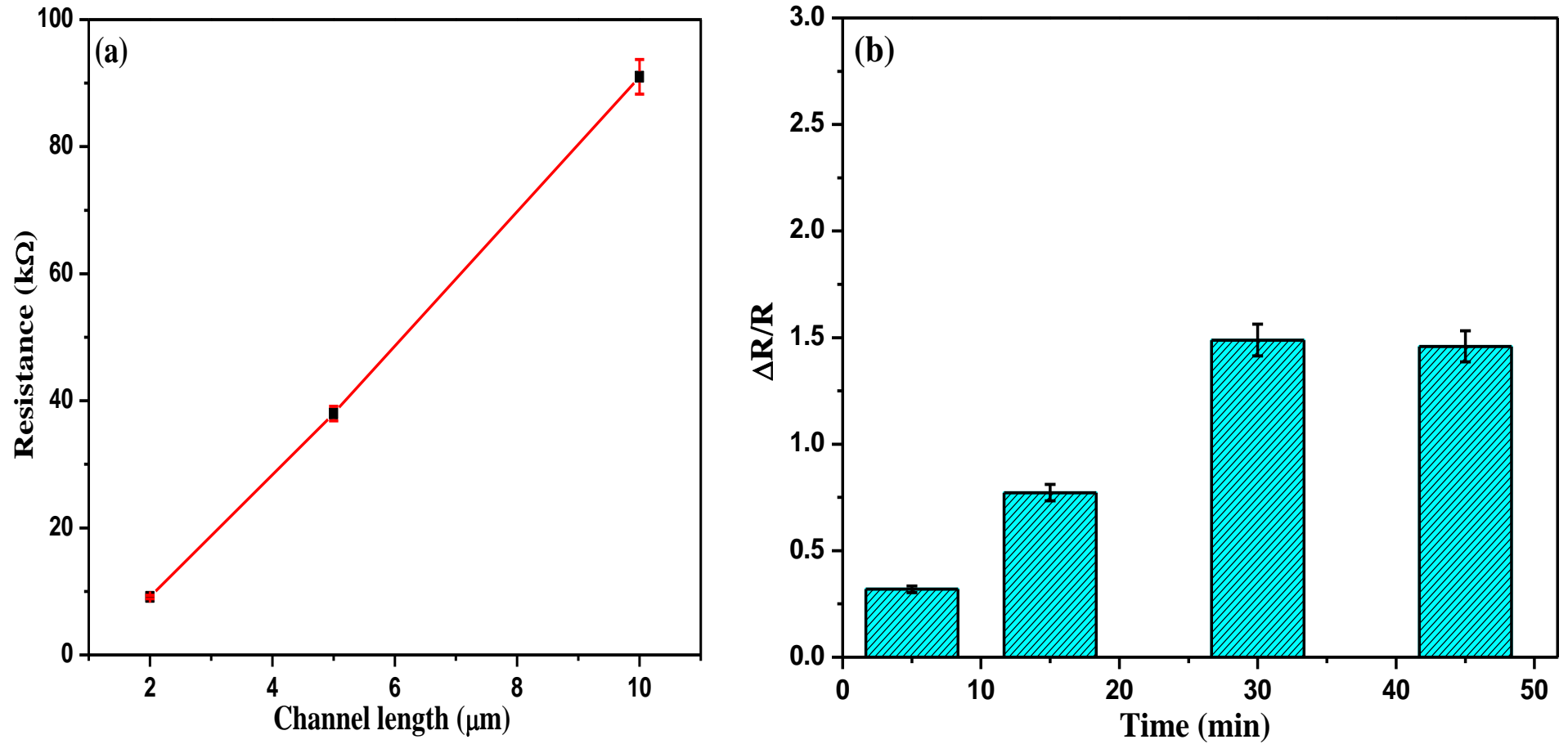


Figure 5

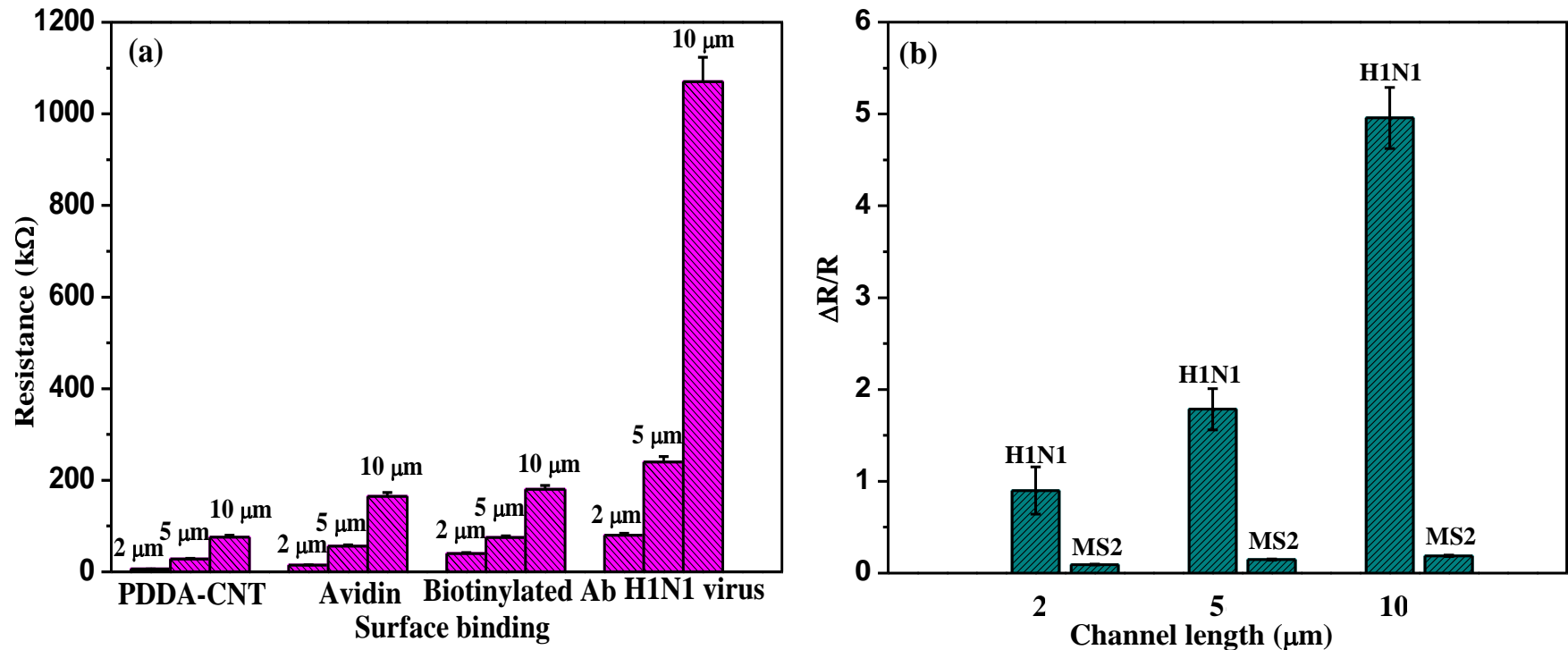


Figure 6

